REDESIGN OF LARGE STEAM TURBINES FOR INCREASED RELIABILITY

by
Malcolm E. Leader
Turbomachinery Consultant
Applied Machinery Dynamics Company
Dickinson, Texas
Randal G. Rials
Senior Reliability Engineer
EquiStar Chemical Company
Lake Charles, Louisiana
and
Charles R. Rutan
Senior Engineering Advisor
EquiStar Chemical Company
Alvin, Texas

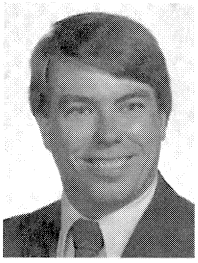

Malcolm E. Leader is a Turbomachinery Consultant and Owner of Applied Machinery Dynamics, in Dickinson, Texas. He is currently involved in the design, testing, modification, and installation of rotating equipment. He spends time doing theoretical design audits and working in the field implementing changes and overseeing installations.

Mr. Leader obtained his B.S. (1977) and M.S. (1978) degrees from the University of Virginia. While there, he worked extensively on experimental rotordynamics and hydrodynamic bearing design. He has written several papers on the subjects of experimental rotordynamics, bearing design, design audits for rotating equipment, and practical implementation of rotordynamic programs. Mr. Leader is a member of ASME, Sigma Xi, the Houston Chapter of the Vibration Institute, and is a registered Professional Engineer in the State of Texas.

Randal G. (Randy) Rials is Senior Reliability Engineer for EquiStar Chemical Company, in Lake Charles, Louisiana. His experience has been concentrated in the areas of maintenance, reliability, and troubleshooting of rotating equipment in the Ethylene Unit at the Lake Charles facility for the past 10 years. Before joining EquiStar Chemical, he was with the Strategic Petroleum Reserve for five years where he served as a Maintenance Engineer.

Mr. Rials received a B.S.M.E. degree (1983) from McNeese State University.

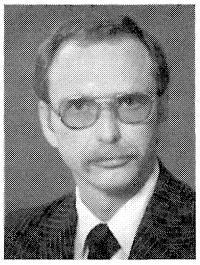

Charles R. (Charlie) Rutan is an Engineering Fellow for OxyChem Petrochemicals Group at the Chocolate Bayou facility in Alvin, Texas. Initially, he was a Project Engineer for Monsanto Company, then moved into equipment specification, installation, startup, and problem solving. After Monsanto, Mr. Rutan worked for Conoco Chemicals, DuPont, and Cain Chemicals. He was a Mechanical Area Maintenance Manager at the Chocolate Bayou facility prior to being promoted to his present position.

Mr. Rutan received his B.S. degree from Texas Tech University (1973). He was appointed to the Texas Tech University Department of Mechanical Engineering Academy of Mechanical Engineers and is a member of the Turbomachinery Symposium Advisory Committee. He has been active in ASME, the Turbomachinery and the International Pump User's Symposia, the Southern Gas Compression Conference, the Hydraulic Institute, and AIChE.

ABSTRACT

Two similar large steam turbines in an ethylene plant are profiled. One drives the cracked gas compressor train and the other drives the propylene refrigeration compressor. The two machines are similar and this paper concentrates on the turbine driving the cracked gas compressors. Both turbines had a history of high vibration, short bearing life, and unusual sensitivity to thermal changes and imbalance due to operation near the second critical speed. In addition, numerous blade failures had occurred. When additional turbine performance was required, a complete review of the entire turbine including the blade designs, rotordynamics, and governor operation was commissioned. The performance upgrade included new blading, disks, seals, and other changes to the steam

path. A turning gear was added for slow-roll operation to relieve thermal effects and rotor bow. A technique was developed for mounting the turbine disks on the rotor to minimize axial disk runout and local couple imbalances.

The high bearing temperatures and high vibration issues were addressed with changes in shaft and bearing designs. A submerged arc welding process increased the governor end journal diameter from 5¼ inches to 7 inches. A rotordynamic optimization analysis resulted in replacing the tilting pad bearing on the governor end with an offset-half lobed journal bearing. The tilting pad bearings on the exhaust end of the turbines were retained but redesigned for optimum performance. Interchangeability of bearings between the two machines was maintained.

These shaft and bearing changes resulted in a significant reduction in babbitt temperature, shaft vibration, and imbalance sensitivity as well as control of the second critical speed. The interaction of the rotor with the foundation substructure was found to be significant, and its inclusion in the analysis was required to properly design the optimized bearings. The blade design changes and steam path changes produced a more reliable design and greater than the required extra power. The addition of a turning gear drive has eliminated the thermal bow problems. A new electronic governor system has eliminated the wear associated with the original hydraulic governor. Both turbines are now operating very smoothly at the capacity of the production facility.

INTRODUCTION

Commissioned in the early 1970s, this olefins plant has been expanded and rerated several times. Blade failures occurred twice in the steam turbines driving the cracked gas compressors and the propylene refrigeration compressor. Root-cause analysis determined that excessive centrifugal stress and improper machining techniques were the reasons for the blade failures. The governor system of each turbine also failed three times, causing complete unit shutdown and significant production losses. Since the turbines had no turning gear drives, thermal bowing of the rotors was a recurring problem, often causing many hours of slow-roll operation to relax the rotor "bow" before each restart. This procedure resulted in material flaring and additional losses. Figure 1 is a photo of the governor end of the cracked gas installation. A number of new features can be seen including the turning gear assembly and the redundant electronic governor probes. Figure 2 is a photo showing the propylene refrigeration train. A composite CAD drawing of the two turbine rotors, detailed in Figure 3, shows that the differences are primarily in the condensing section wheels.

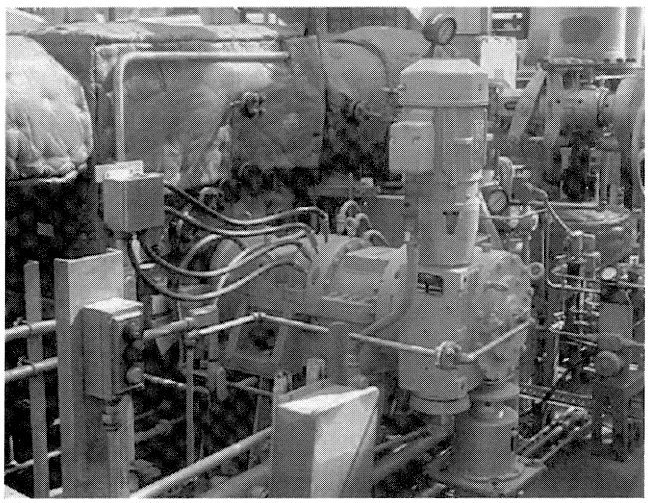

Figure 1. Governor End of Cracked Gas Steam Turbine.

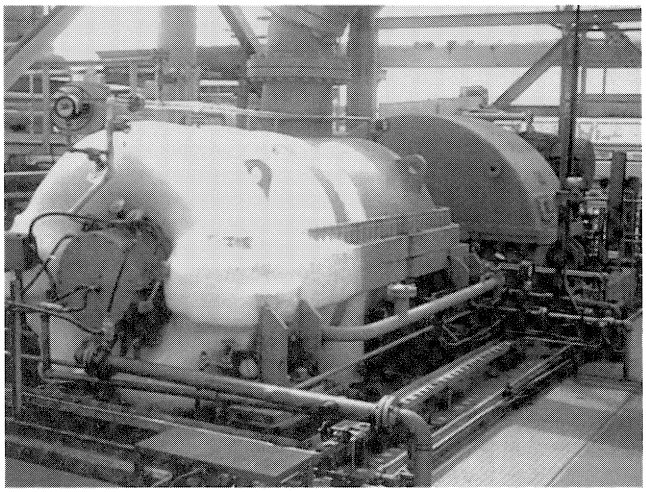

Figure 2. Propylene Refrigeration Train.

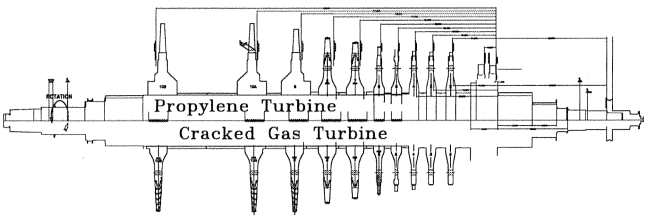

Figure 3. Composite Drawing of Both Steam Turbine Rotors.

In 1992, an internal inspection showed blade failures of the sixth and last stage blades of one turbine. Failure analysis revealed that the stresses on the sixth stage blades were too high, and the roots of these blades were redesigned to withstand the imposed loads. The last stage blades had failed where the lashing wire pierced the blade due to stress risers left from the machining operation that made the holes in the blades. The stress risers were removed and later the blading was redesigned to eliminate the lashing wire and a shrouded blade type was used.

The hydraulic governor was originally driven through a spline coupling to a gear that drove the governor. Several attempts were made to strengthen the spline coupling, but failures persisted. High vibration also caused deterioration of the gear teeth and several failures of the drive mechanism. The decision was made to eliminate the mechanical aspect of the governor drive and add a completely electronic governing system with redundant speed pickup sources and power control backup.

The two drive turbines were modified for increased horsepower in 1985, and the journal bearings were redesigned as seven-pad tilting pad bearings. Unfortunately, these modifications failed to increase the bearing reliability as desired. The primary bearing problem in these machines is excessive loading on the steam end bearing causing high temperatures and high babbitt loads. The existing geometry was a 5¼ inch diameter, seven-pad tilting pad bearing supporting the 5474 lb journal load. The pads were 3 inches long, which yields a static unit loading $\left(\frac{W}{LD}\right)$ of 348 psi. A typical conservative design limit is 200 psi. Since the pads were only ¾ inch in thickness, the seven-pad design was used to minimize pad bending due to the rotor gravity load. Pad bending increases effective pad preload, which increases the bearing stiffness.

For the original seven-pad bearings, the calculated peak hydrodynamic pressure (*without* any alternating forces from vibration) is over 1370 psi. This is well above normal design, which is generally limited to less than 1000 psi in this type of machine unless special precautions are taken. The calculated minimum oil film thickness in this bearing is only 0.7 mils at the

5248 rpm design speed. The predicted maximum babbitt temperature was 210°F, which is higher than desired for a bearing in this service. Actual operating temperatures were 210°F to 220°F, which reduces the margin of safety and causes higher than desired alarm and shutdown limits.

SHAFT AND BEARING REDESIGN

In order to increase the load support area of the steam end bearing, an increase in shaft diameter from 5¼ inches to 7 inches was proposed. Figure 4 is the original proposal of a shrunk-on sleeve to increase the journal diameter. This diameter increase was actually achieved by a submerged arc welding process, which is a better solution. The axial length of the bearing could not be significantly increased due to space limitations in the case. The change in diameter alone reduced the specific loading from 348 psi to 261 psi, a 25 percent decrease.

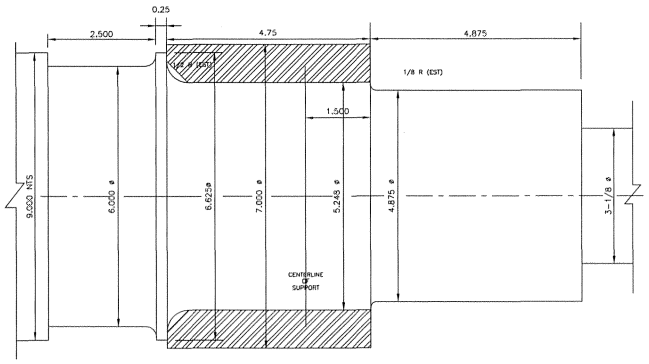

Figure 4. Proposal to Increase Journal Diameter with Shrunk-On Sleeve.

Space constraints in the steam end bearing housing limit the use of a tilting pad bearing with the larger 7 inch diameter journal. The pads would have been too thin to resist the journal load without significant bending. A gravity load-on-pad orientation could have been made to fit, but the unit hydrodynamic loading would have exceeded 1000 psi. Thus, an optimized fixed-geometry sleeve bearing at the steam end was designed. Several bearing geometries were considered including a plain elliptical profile, a pressure dam type, and multilobe designs. After comparing many factors, the recommended geometry was an offset-half profile having a 4 inch axial length, a bore clearance of 0.018 inch, and a set clearance of 0.009 inch (diametral). This results in a preload of 50 percent, and an offset factor of 1.0, which means the minimum clearance is at the trailing edge of the pad. This design yields two open-mouth converging oil wedges, as shown in Figure 5. This bearing is easy to manufacture, provides ample damping, and resists subsynchronous whirl. The static unit loading is reduced to 196 psi, a comfortable level, with much lower peak hydrodynamic loading (720 psi) at-speed. In addition, the predicted maximum babbitt temperature drops 30°F at full speed. Predicted vibration levels due to imbalance also decrease and the stability margin increases.

On the exhaust end, the original 7 inch diameter journal is retained. Here, the seven-pad bearing was replaced by a five-pad, load-between-pad, tilting pad bearing. The original 4 inch axial length is acceptable. The preload was reduced from the original 40 percent to a maximum of 18 percent and the nominal set (pivot) clearance is changed to 14 mils diametral. The new five-pad design (Figure 6) lowers the exhaust end peak hydrodynamic loading from 775 psi to 680 psi, with corresponding reduced temperatures and increased effective damping.

The analysis began by producing accurate computer models of the rotor, the support pedestals, and the existing bearings. Undamped critical speed mode shapes, the damped unbalance response, stability, and bearing temperatures were calculated for

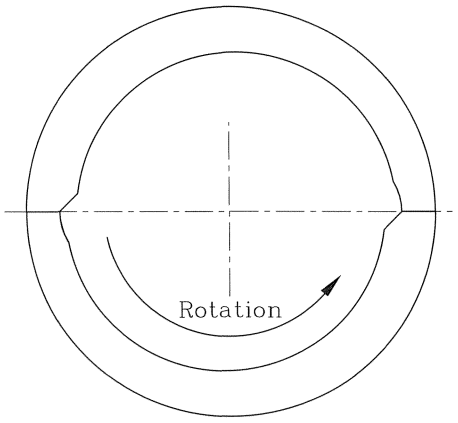

Figure 5. Offset-Half Journal Bearing Cross Section.

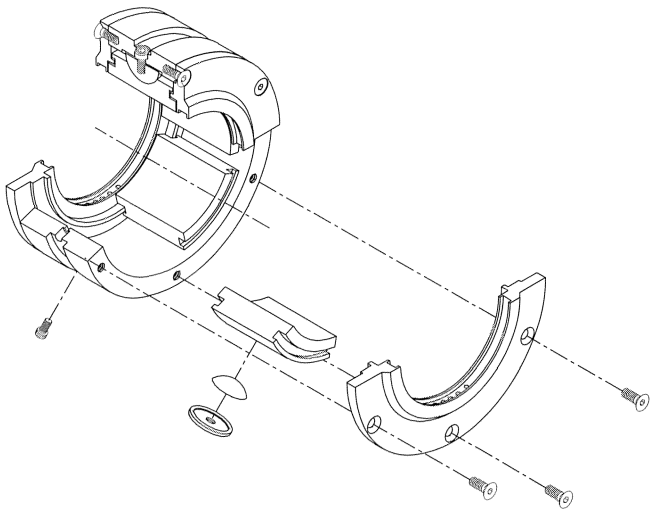

Figure 6. Exploded View of Five-Pad Tilting Pad Bearing. (Courtesy of Turbo Components and Engineering, Inc.)

the existing configuration. Then many other bearing designs of varying geometries were evaluated and compared until an optimized replacement bearing configuration for each end of the rotor was found.

Rotor Model

The computer representation of the steam turbine rotor was developed from OEM drawings, field measurements, and documentation. All critical dimensions are matched and verified at this point before the analysis proceeds. This rotor consists of a solid forging with the first compound stage and the next three Rateau stages as integrally forged wheels with attached blading. Stages 5 through 10 are fixed by keyed and shrunk-on disks with spacer sleeves between stages. The overall rotor length is 163.76 inches including the bolted-on thrust collar assembly. For the analysis, only the shaft itself was considered, which has an overall length of 158⅜ inches. All attachments to the rotor including disks, sleeves, and blades were applied as lumped masses and inertias. The bearing centerline distance is 131⅜ inches. Midspan shaft diameter is 13.172 inches. The flexible shaft coupling is a diaphragm type with a half-weight of 138.8 lb at 3⅛ inch from the end-of-shaft. As a conservative measure, no external stiffening due to shrink fits is allowed, due to the relief of this pressure from centrifugal force at speed.

Illustrated in Figure 7 is the computer section model developed to compute lateral critical speeds, unbalance response, and rotordynamic stability. The model consists of 42 rotor sections

with a single-level lumped-parameter pedestal model at each bearing location. The outlined sections represent blade rows where the mass and inertia are added.

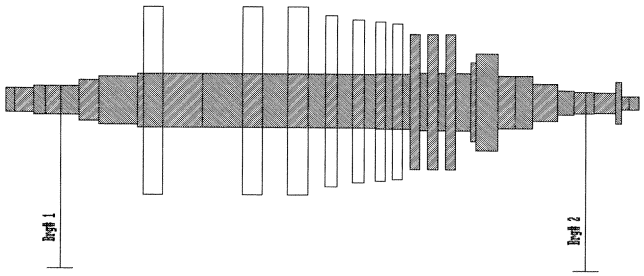

Figure 7. Computer Model of Cracked Gas Steam Turbine.

Bearing Pedestal Model

Mass and stiffness properties for the bearing support pedestals were estimated from experience with other turbines of similar size and design. There are more exact ways of characterizing the pedestal stiffness and damping through modal testing or finite element modeling. However, this method was found to be adequate for this evaluation. The values used are listed in Table 1. Pedestal damping values were set to 10 percent of critical damping. Critical damping is defined as:

$$C_C = 2\ m\ \omega_n \tag{1}$$

where:

m = Pedestal effective dynamic mass = weight/386.088, lb_f-sec^2/in
ω_n = Pedestal natural undamped resonance, rad/sec

Table 1. Bearing Pedestal Characteristics.

Pedestal Location	Weight (lbm)	Horizontal Stiffness (lbf/in)	Vertical Stiffness (lbf/in)	Horizontal Damping (lbf-sec/in)	Vertical Damping (lbf-sec/in)
Steam end	500	1.5×10^6	3.0×10^6	279	394
Exhaust end	500	1.5×10^6	3.0×10^6	279	394

UNDAMPED CRITICAL SPEED ANALYSIS

The undamped critical speed analysis was performed to visualize the rotor mode shapes at critical speeds and to produce a critical speed map. Actual critical speed rpm values are *not* predicted by this stage of the analysis. The rotor deflected shape is used to understand the dynamic behavior at critical speeds, to guide in the placement of imbalance during the damped response analysis, and to evaluate the severity of vibration amplitudes at axial locations other than the proximity probe. The horizontal (*Kxx* and *Cxx*) and vertical (*Kyy* and *Cyy*) bearing stiffness and damping values are used to calculate effective dynamic stiffnesses by the following equations:

$$K_{dx} = \sqrt{(Kxx)^2 + (\omega Cxx)^2} \tag{2}$$

and:

$$K_{dy} = \sqrt{(Kyy)^2 + (\omega Cyy)^2} \tag{3}$$

where:

$$\omega = \frac{2\pi \times rpm}{60} \quad \frac{rad}{sec} \tag{4}$$

This allows for the bearing damping to be included as a dynamic effect in the undamped analysis. Only the K_{dy} stiffness values were used to produce the mode shape plots, since the stiffest direction bearing coefficients will usually dominate the rotor behavior.

Figure 8 is an "animated" plot of the first vertical undamped critical speed mode shape with original bearings. This figure shows that this mode is cylindrical and that the maximum amplitude occurs near the rotor center. There are node points just outboard of each bearing and the relative amplitudes at the bearings are low, which indicates that bearing damping will be ineffective. Reducing the vertical bearing stiffnesses is a way to alleviate this problem.

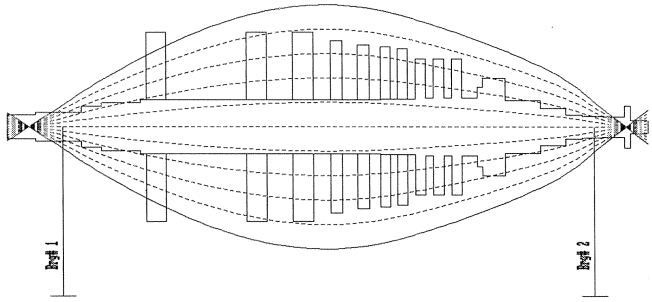

Figure 8. First Critical Speed Undamped Mode Shape.

Figure 9 shows the second vertical mode shape as pivotal with a node point near midspan. The relative amplitude at the bearings is high so the bearing damping should be effective in controlling this resonance. The thrust end of the rotor is more rigidly restrained as indicated by the bending of the mode shape. This means that the governor end bearing is probably too stiff for this application.

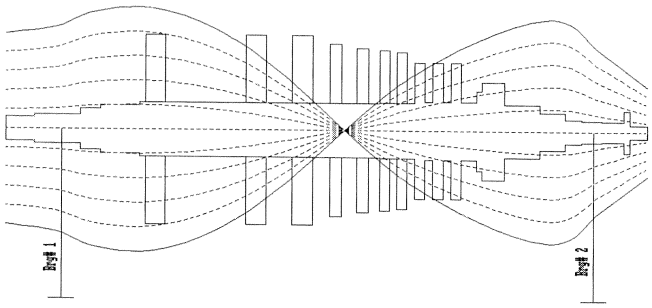

Figure 9. Second Critical Speed Undamped Mode Shape.

The critical speed map, shown in Figure 10, is an important tool that plots the first three critical speeds as a function of bearing stiffness. This log-log presentation shows all possible values of the first three critical speeds for this rotor for bearing stiffnesses ranging from 10,000 lb/in (very soft) to 10,000,000 lb/in (extremely stiff). The first two critical speeds are zero at zero support stiffness while the third critical speed, the first bending mode, is a "free-free" mode and has a zero stiffness frequency near 6000 cpm.

The first critical speed is below 1000 rpm when the bearing stiffness is less than 200,000 lb/in. This resonance frequency increases as stiffness increases until it reaches 2140 rpm, when the bearing stiffnesses are 10,000,000 lb/in each. The second critical speed and the third mode also increase in frequency as the bearing stiffnesses increase. Also on this plot are the (average of steam end and exhaust end) dynamic stiffness values (defined above) for the original bearings and the proposed optimized bearings. The original bearings have very high dynamic vertical stiffness.

In the vertical direction, the proposed replacement bearings have a much lower dynamic stiffness than the existing bearings. This decreased vertical stiffness results in an increase in relative vertical

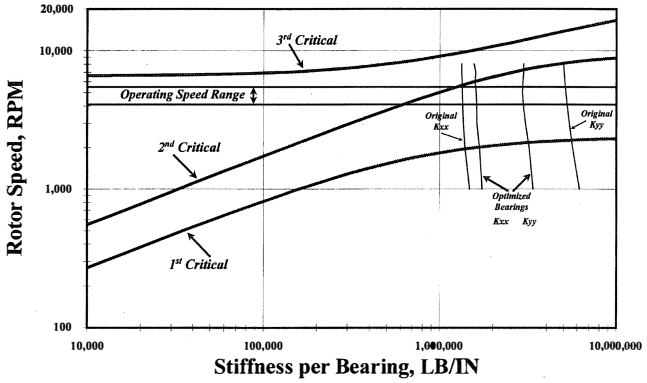

Figure 10. Steam Turbine Rotor Undamped Critical Speed Map.

modal amplitude at the bearings. The effective bearing damping increases as the relative bearing amplitude increases. The expected result is decreased vibration amplitude as effective damping dissipates the vibration energy. In the horizontal direction, the new bearings show slightly higher dynamic stiffness than the old bearings. The operating speed range, given as 4315 rpm to 5394 rpm, is plotted and indicates a potential interference with the second critical speed in the horizontal direction.

BEARING PROPERTIES

The recommended steam end replacement bearing is an offset-half design (Figure 5). This bearing is a simple two-lobe design with minimum clearance at the trailing edge (100 percent offset). The leading edge of each pad has the greatest clearance and induces a good supply of cool fresh oil at all times. The tight clearance at the trailing edge of each pad helps increase the horizontal stiffness and produces a more symmetric design. The primary disadvantage is that the offset-half bearing is not designed for high-speed reverse rotation. Care must also be exercised to assure the bearings are properly installed. This configuration is relatively easy to manufacture and retrofit to this machine.

Figure 11 is a comparison of the horizontal and vertical stiffness between the original seven-pad bearing and the offset-half design. Due to the increased diameter and length, the vertical stiffness has been significantly reduced, which will aid in improving effective modal damping.

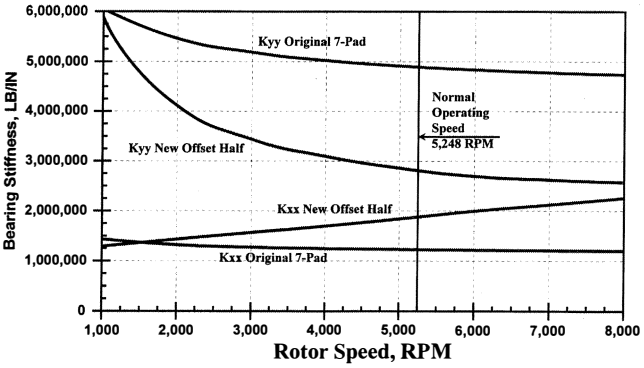

Figure 11. Comparison of Principal Stiffnesses—Seven-Pad Versus Offset-Half Governor End Bearing.

The offset-half bearing does produce cross-coupled stiffness and damping, which has little effect on synchronous vibration but can contribute to subsynchronous (unstable) rotor motion. However, if this destabilizing effect is countered by an increase in positive damping effects, the net effect can be to increase stability. While tilting pad bearings have such low cross-coupling, it is generally ignored. It can be calculated and was included in this analysis. The cross-coupled coefficients of the two different bearings are plotted in Figure 12. A significant bearing characteristic change for the steam end bearing redesign is indicated in Figure 13, the damping comparison. The offset-half bearing horizontal damping is more than double the seven-pad design, and the vertical damping is increased by more than three times.

On the exhaust end of the machine, a five-pad, load-on-pad design offers improvement over the existing seven-pad bearing without sacrificing anything to pad deflection. Figure 14 shows that the vertical stiffness is reduced with the five-pad design, again allowing for more effective damping in this plane. The horizontal stiffness increases to produce a more symmetrical design. The new exhaust end five-pad bearing damping comparison is shown in Figure 15. While the damping is reduced with the five-pad design, the corresponding stiffness reduction results in an increase in effective damping.

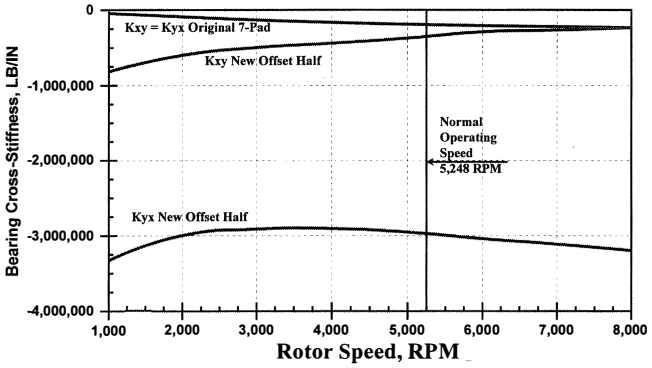

Figure 12. Comparison of Cross-Coupled Stiffnesses—Seven-Pad Versus Offset-Half Governor End Bearing.

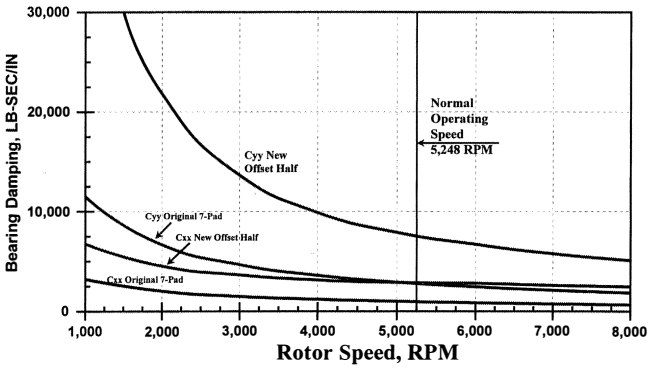

Figure 13. Comparison of Principal Damping—Seven-Pad Versus Offset-Half Governor End Bearing.

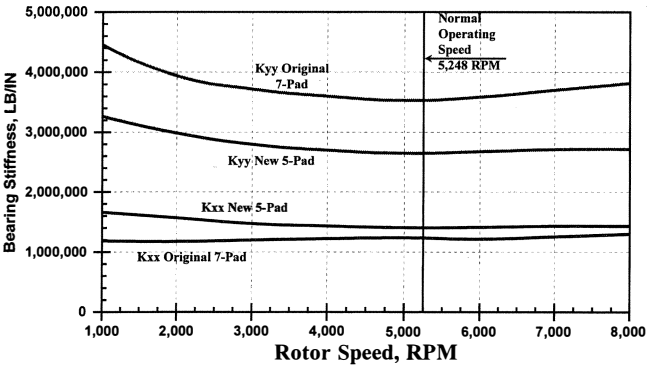

Figure 14. Comparison of Principal Stiffnesses—Seven-Pad Versus Five-Pad Exhaust End Bearing.

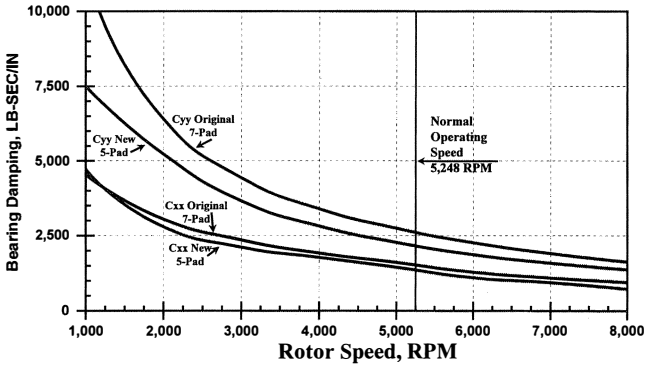

Figure 15. Comparison of Principal Damping—Seven-Pad Versus Five-Pad Exhaust End Bearing.

One of the major advantages to the new offset half design on the steam end is the reduced peak hydrodynamic loads from 1370 psi to 720 psi. This is also reflected in reduced babbitt temperatures. Figure 16 shows that above 2200 rpm, the offset half design produces significantly reduced babbitt temperatures up to 30°F at the normal operating speed. Not only does this help the babbitt fatigue strength, but the oil film viscosity is increased, which also improves the damping. The five-pad exhaust end bearing reduces maximum pad temperature by 9°F, as shown in Figure 17. The reduced temperatures can only have a positive affect on bearing life.

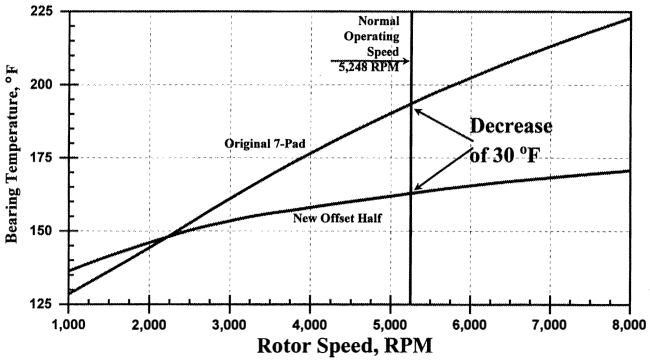

Figure 16. Comparison of Pad Temperature—Seven-Pad Versus Offset-Half Governor End Bearing.

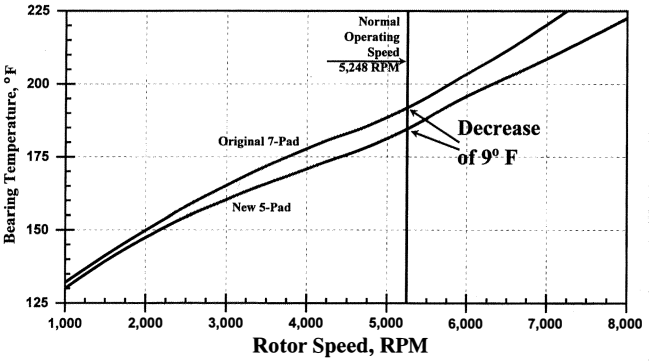

Figure 17. Comparison of Pad Temperature—Seven-Pad Versus Five-Pad Exhaust End Bearing.

DAMPED UNBALANCE RESPONSE

This portion of the analysis simulates the effect of placing a known synchronous imbalance forcing function on the rotor and calculating the vibration amplitude at the probe locations. The amount of imbalance chosen is the API limit of 4 W/N, where W is the rotor weight in pounds and N is the speed in rpm. The units of this imbalance are in ounce-inches. This rotor weighs 11,100 lb, so at 5248 rpm the 4 W/N value is 8.46 oz-in. For this analysis, this amount was placed at stage 8 (midspan) on the rotor at 0 degrees relative phase. Simultaneously, 2 W/N was placed on the rotor ends at 90 degrees and 270 degrees to excite the second mode. Combining these three imbalances simulates typical field situations.

Using all speed-dependent bearing stiffness and damping coefficients, the rotor speed was varied from 1000 rpm to 8000 rpm and the maximum amplitude at each probe location was calculated. Only the nominal clearance and preload values were used when calculating the bearing coefficients. In addition, a casing substructure model (detailed above) was included in the analysis to obtain more accurate results. The calculated peak-to-peak amplitudes are the relative motion between the shaft and the casing, just as the actual displacement probes "view" the shaft.

Figure 18 is the comparison of the predicted maximum relative displacement on the steam end with the original and replacement bearings. Both the first and second critical speeds are "split," due to the asymmetry in the bearing stiffness and the pedestal characteristics. The reduction in amplitude with the optimized bearings is significant throughout the speed range. Due to an increase in available damping, the critical speed peak amplitudes are significantly reduced, but the amplitude at 5248 rpm is only reduced by 18 percent. The actual measured governor end vertical vibration from a solo coastdown is plotted in Figure 19. While the predicted and actual response plots do not correspond directly, there is good agreement considering the actual rotor imbalance distribution is not known.

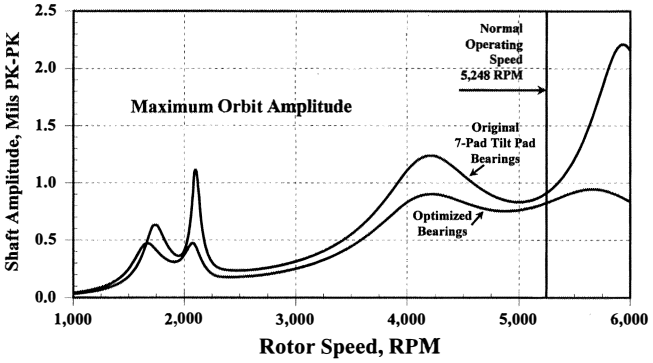

Figure 18. Predicted Unbalance Response—Governor End Maximum Orbit Amplitude.

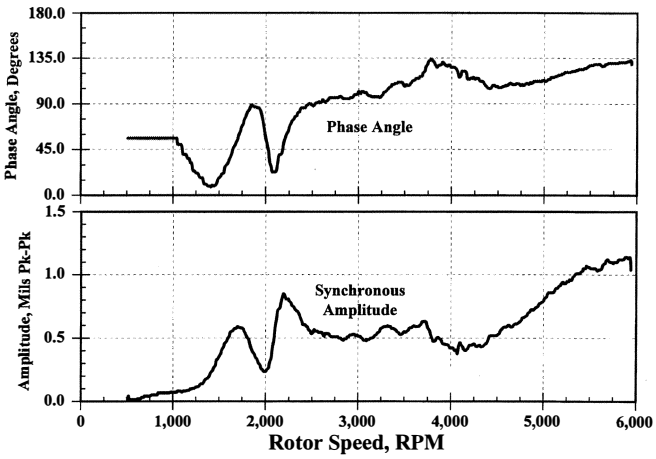

Figure 19. Actual Synchronous Response—Solo Rundown—Governor End Vertical Amplitude and Phase.

The midspan rotor motion for the two cases is compared in Figure 20. Here there is a dramatic reduction in amplitude at the first critical with a 66 percent reduction in maximum shaft vibration. This will significantly reduce the possibility of rubs while passing through the 2000 rpm to 2250 rpm speed range. Installed field data are not available for the midspan location.

The predicted exhaust end maximum probe relative displacement comparison is shown in Figure 21. The reduction in amplitude at all speeds with the optimized bearings is again substantial with a 33 percent decrease at 5248 rpm. Figure 22 is the actual response taken from the exhaust end vertical vibration probe. Again the agreement between predicted and actual response is quite good.

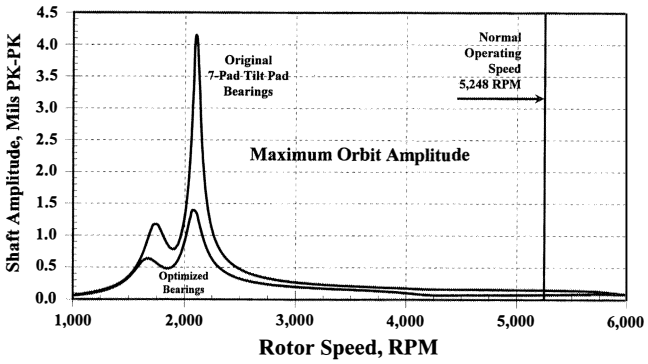

Figure 20. Predicted Unbalance Response—Midspan Maximum Orbit Amplitude.

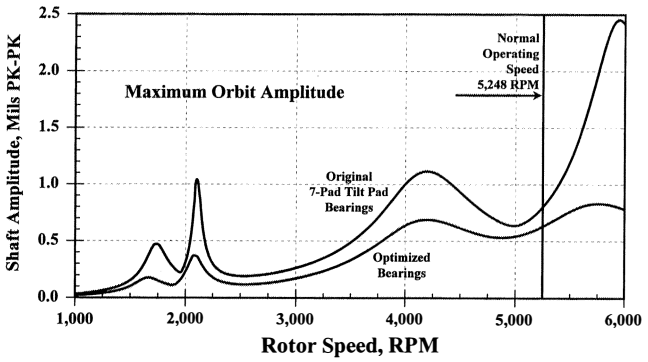

Figure 21. Predicted Unbalance Response—Exhaust End Maximum Orbit Amplitude.

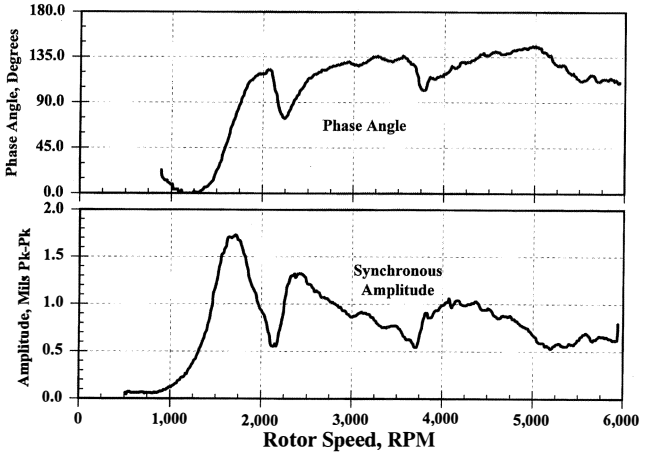

Figure 22. Actual Synchronous Response—Solo Rundown Exhaust End Vertical Amplitude and Phase.

The dynamic amplification factor of a critical speed is defined by API specifications (API 684, 1996) as:

$$AF = \frac{N_{CR}}{N_2 - N_1} \tag{5}$$

where:

N_{CR} = Rotor speed at maximum amplitude (rpm)
N_1 = Rotor speed below critical at 0.707 × maximum amplitude (rpm)
N_2 = Rotor speed above critical at 0.707 × maximum amplitude (rpm)

Table 2 lists the reduction in amplification factors for the governor end first and second critical speeds when the optimized bearings are used. Unfortunately there are no data available to measure the actual original amplification factors. The measured amplification factors with the optimized bearings are lower than the predicted amplification factors. Table 3 lists similar data for the exhaust end bearing.

Table 2. Governor End Amplification Factor Summary.

Critical Speed Mode	Governor End Amplification Factor ORIGINAL BEARINGS	Governor End Amplification Factor OPTIMIZED BEARINGS		Predicted Percent Reduction
		Predicted	Actual	
First mode horizontal	10.3	7.7	5.3	25
First mode vertical	37.4	16.0	6.1	55
Second mode horizontal	5.4	3.2	N/A	41
Second mode vertical	12.7	5.0	2.5	61

Table 3. Exhaust End Amplification Factor Summary.

Critical Speed Mode	Governor End Amplification Factor ORIGINAL BEARINGS	Governor End Amplification Factor OPTIMIZED BEARINGS		Predicted Percent Reduction
		Predicted	Actual	
First mode horizontal	10.4	7.7	4.4	26
First mode vertical	36.0	17.7	3.6	51
Second mode horizontal	5.8	4.2	3.5	27
Second mode vertical	12.9	5.1	N/A	60

ROTOR STABILITY

The susceptibility of any rotor bearing system to develop subsynchronous vibration can be determined by calculating the logarithmic decrement (or log dec). This dimensionless quantity is the vibration decay factor. When positive, the subsynchronous vibrations are suppressed and the more positive the log dec is, the greater the stability. If the log dec becomes negative, subsynchronous vibrations are not suppressed and these vibration components may be present.

Aerodynamic cross-coupling is a destabilizing forward whirl mechanism present in all machines from the interaction between the fluid (steam) and the rotating components. Cross-coupling effects from all sources including the blades, seals, and bearings, combine with the available damping to determine the net machine stability. The aerodynamic cross-coupling in a compressible-flow machine may be estimated as a function of the stage torque and blade geometry (approximately) by the Alford equation:

$$K_{xy} = -K_{yx} = \frac{\beta T}{2Rh} \tag{6}$$

where:

T = Blade row torque (lb_f-in)
R = Blade mean radius (in)

h = Blade axial length at tip (in)
β = Cross-coupling factor (≈6 for a steam turbine)

For the 31,900 hp turbine running at 5248 rpm with the cross-coupling divided evenly over the seven large blade rows, the cross-coupling per row becomes:

$$K_{xy} = -K_{yx} = \frac{1}{7}\frac{6\,(383{,}098\ \text{lbf-in})}{(2)\,(20\text{in})(2\text{in})} \qquad (7)$$

$$= 4{,}105\ \text{lbf/in (per blade row)}$$

Adding in cross coupling from labyrinths, the estimated cross-coupling is approximately 5000 lb_f/in per stage. This is consistent with experience and published values for similar machines.

In Figure 23, the calculated log dec is plotted as a function of speed for the original bearings with no cross-coupling and for the case of 5000 lb_f/in/stage. The log dec values calculated for the optimized bearings are also shown. All cases are stable, but with the estimated aerodynamic forces applied, the seven- pad bearings produce a very low log dec. With the new bearings, the stability is increased significantly.

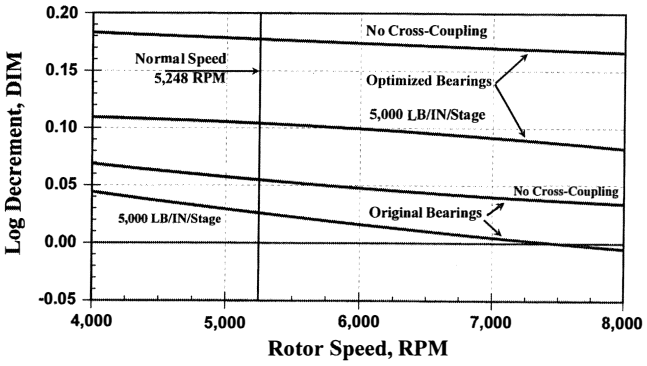

Figure 23. Stability Comparison—Logarithmic Decrement Original Versus Modified Configuration.

MOUNTING OF TURBINE DISKS

The turbines in this analysis have seven disks or wheels mounted on the shaft, secured by single keys. It is important whenever shrink fits are used to provide adequate torque-carrying capability and enough holding power to keep the disks from moving axially over time, sometimes called "walking" disks. The centrifugal forces expand the bore of each mounted disk and relieve the shrink pres-sure. The larger the ratio between the disk outside diameter and inside diameter, the more bore growth from centrifugal force. This reduces the shrink pressure and thus the torque capacity and may increase the chance of axial disk movement. Too much shrink pres-sure can result in forces in excess of material yield and could lead to permanent deformation (yielding) or disk failure. It is important to provide the right amount of interference for any mounted disk or wheel.

Most turbine disks and compressor wheels have complex geometries and cannot be treated as plain disks directly. Actual values will not be calculated here for the wheels on these turbines since they are not plain disks. However, a good feel for the shrink pressures, bore expansion, and torque capacity can be achieved by examining what happens when a plain disk is shrunk onto a shaft. All calculations in this section apply only to steel-on-steel fits. Figure 24 is a plot of shrink pressure, in psi, as a function of interference ratio. Interference ratio (I_R) is the inches of interference per inch of shaft diameter. Mils per inch is 1000 times the interference ratio applied here. The equations used here were derived from Juvinall (1967) and Young (1989). Three curves are shown for different disk outside diameter to bore ratios. As the outside diameter approaches the bore diameter, the shrink pressure is relieved. As the disk diameter becomes very large compared with the bore, the shrink pressure asymptotically approaches:

$$P_s = \frac{I_R\,E}{2} \qquad E = \text{Modulus of Elasticity} \qquad (8)$$

It is important to note that 2 mils-per-inch is not excessive shrink pressure even for the case of a large diameter ratio disk, as long as high yield materials are used. In some cases, temperature differential bet-ween the disk and the shaft will also affect the actual net shrink pressure.

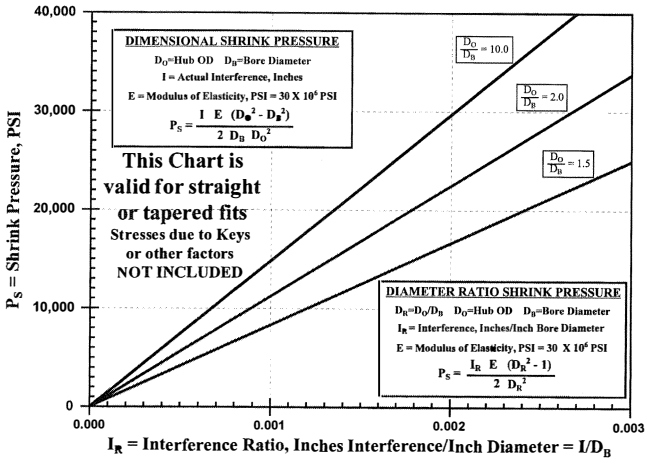

Figure 24. Shrink Pressure Versus Interference Ratio for Various Disk Diameter Ratios.

The torque capacity of a shrink fit can be calculated as shown in Figure 25. This chart is for the case of 2 mils-per-inch interference (at-speed) and various bore diameters. Several assumptions have been made including the friction coefficient (0.15) and an effective length equal to 50 percent of the bore diameter. The actual effective length is a function of how good the fit is between the disk and the shaft. Typical fits have an actual effective length of 30 percent to 70 percent of the bore. Long shrink fits are often relieved over part of the fit, so the construction details must be known. The effective length required to carry a given torque can be calculated from this chart. Unintended tapers or out-of-round conditions of shrink fit joints are a particular problem and must be corrected for a designed connection to carry the torque required.

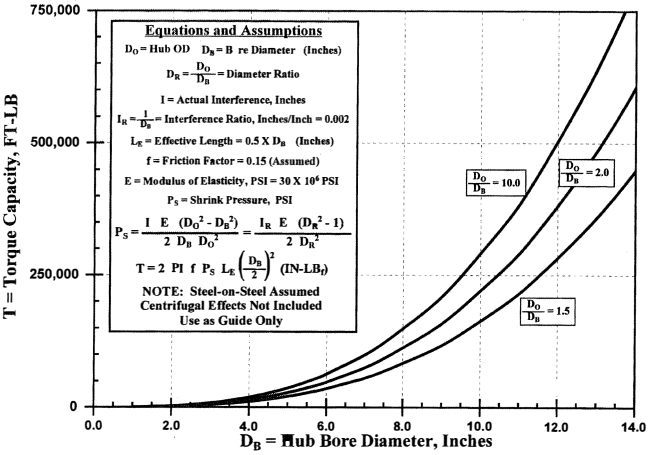

Figure 25. Torque Capacity Example for Two Mils-Per-Inch Shrink Fit of a Plain Steel Disk on Steel Shaft.

Centrifugal force from rotation causes expansion of the bore of a mounted disk and, to a lesser extent, the shaft. This differential relieves the shrink pressure and reduces the torque capacity. Figure 26 is the bore expansion of a plain disk as a function of speed for various disk dimensions. Figure 27 relates this bore expansion to shrink pressure relief ignoring the shaft dimensional change, which is usually very small. The general trend shows that large diameter disks will have a much greater bore expansion and shrink pressure relief than smaller diameter disks with the same outer diameter to bore ratio. Thus, it becomes apparent why most turbine disks are profiled to remove much of the mass away from the center of the disk. Figure 3 showed that the mounted disks are all profiled on the rotor in this study.

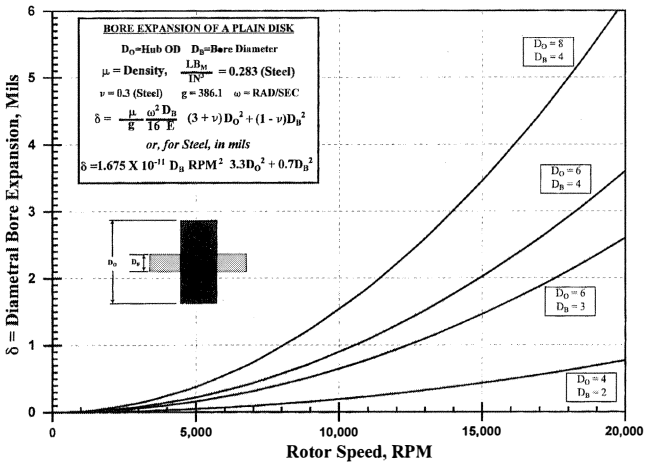

Figure 26. Bore Expansion of Various Plain Disk Sizes as a Function of Rotational Speed.

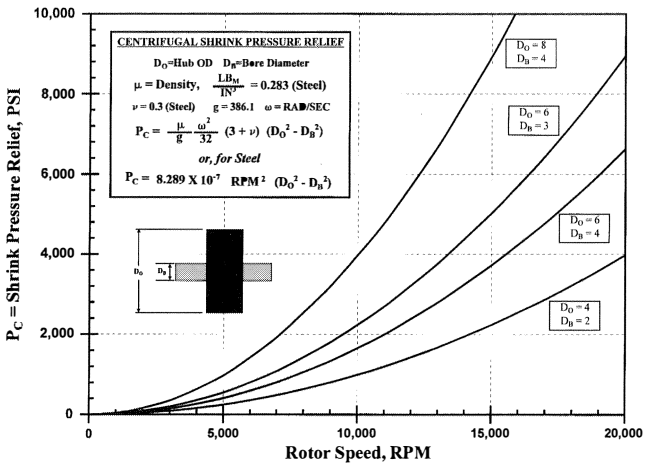

Figure 27. Shrink Pressure Relief Due to Bore Expansion from Centrifugal Force.

The best way to calculate the actual stresses and bore expansion of an actual disk is to model the disk with a finite element program. This is particularly necessary when keyways are cut into the disk, as a keyed shrink fit always has the maximum stress at the bottom of the keyway and the keyway locally relieves the shrink pressure. Figure 28 is a closeup of the bore of a typical turbine wheel that has been shrunk on the shaft at 2 mils-per-inch and "spun" up to operating speed. The resultant stress pattern shows reasonable stresses on the bore and high stresses at the bottom of the keyway. This helps explain why cracks are sometimes found in this area of a mounted disk.

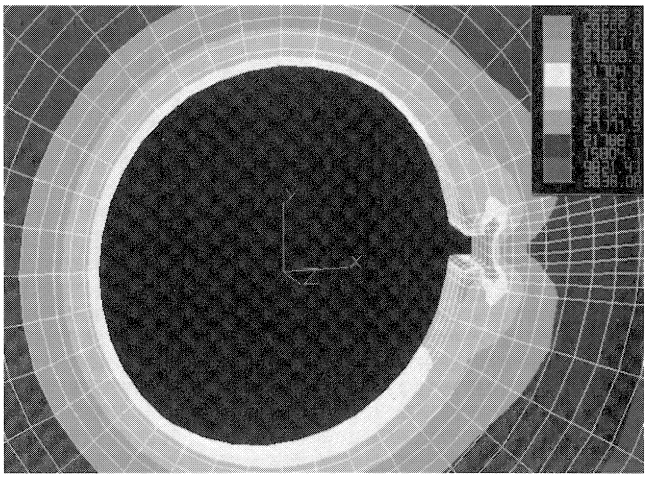

Figure 28. Typical Von Mises Stress Field of a Keyed Shrunk-On Turbine Wheel.

PRACTICAL DISK MOUNTING

Most builtup rotors, such as the ones in this study, are mounted by heating the disk until the bore has expanded sufficiently to allow the disk to be slipped into place where it cools and locks into place. This is not a simple routine, especially with large disks. Many shops have developed fixtures, techniques, and people with experience to be able to mount shrunk-on disks properly. Usually, the original equipment manufacturer (OEM) publishes interference guidelines and tolerances that are followed unless there are known problems with high stresses, failures, disks moving axially, or other problems. In these cases, it is important that a repair shop has the ability (or knows when to seek additional analysis capability) to analyze the fit and adjust it if necessary.

Even with the best conditions, slight disk skew is not uncommon when mounting large diameter disks. Each machine has limits on the axial runout and often disks will have to be removed and remounted if the skew is excessive. This is a time consuming and tedious process, for the assembly must be cooled before the disk can be rapidly heated again to allow the interference to relax and the disk removed. On a machine with many mounted disks, the time and effort to get all the disks on straight may be several days and many man-hours. After each disk is mounted, the rotor must cool and runout values checked to avoid "kinking" the shaft and excessive disk skew. A 3 mil to 5 mil space is normally left between disks and spacer sleeves to allow for thermal growth. It is good practice to check the balance after each disk is mounted, then completely cooled, in what is called a "sequential stack-balance" operation. There are varied opinions as to whether this is even necessary or if two disks can be mounted before a balance check is made. However, it is much easier to correct disk mountings individually than to have to remove six other disks to find the one causing a problem.

One of the biggest problems with skewed disks is that each one introduces a local couple imbalance that is difficult to find and correct. Often the low speed balance correction on a mounted disk will be two weight additions or removals 180 degrees apart on opposite sides of the disk to compensate for the skew. At speed, some disks will straighten, creating a new local couple imbalance. This can lead to a very complex, or even impossible, at-speed balance correction.

This is exactly what occurred with these rotors during the overhaul for shaft modification and reblading. The completely stacked and low speed balanced rotors were placed in a high-speed vacuum pit for at-speed trim balancing. Unexpectedly, step changes in the vibration and phase were observed that were attributed to skewed disks straightening due to centrifugal forces.

This phenomenon introduced enough uncertainty that the rotor was stripped and restacked.

The engineering advisor for the equipment owner developed a straightforward method of mounting and straightening the disks that eliminated the problem. The procedure was normal up to the point of checking the mounted wheel for proper clearance with the adjacent sleeve. Then the rotor was completely cooled to ambient temperature and placed in "V" blocks for runout checks. If the runout measurements were within strict specifications, the mounting process continued. Invariably, the disk skew was excessive and needed correction.

The developed corrective procedure was to spin the rotor at 250 rpm in the balance machine. Then, while monitoring the vibration reading of the balance machine, heat was rapidly applied to the wheel using two "rosebud" torches. As the shrink fit relieves between the disk and shaft, the measured vibration will drop. Then heat is removed with the rotor still spinning. The rotor is allowed to cool to ambient conditions while spinning and the disk will take the proper set, square with the shaft. Rapid cooling can be achieved by blowing air on the rotor during the cooldown. Close attention should be given to sudden temperature changes such as an open door allowing a cold wind to blow on the rotor from one direction. Events like this were observed to cause uneven cooling and additional work straightening the disks and rotor. Once this procedure was completed, the high-speed trim balance succeeded without any problems.

CONCLUSIONS

Two main steam turbines in an olefins plant had experienced numerous failures and unscheduled down time. Several rebuilds and rerates increased the frequency of problems including blade failures, governor drive wear, thermal bows, hot bearings, and high vibration. A systematic approach carefully identified the problems and targeted specific remedies for each problem. The solutions were coordinated into a unified effort applied to the spare rotors and installed during a major planned outage. The blading high stress problems were corrected and an electronic governor was installed that eliminated the mechanical governor drive. A new low speed turning gear mechanism was installed to alleviate thermal bow conditions.

The shaft on the governor end of the rotor was redesigned by increasing the journal diameter and the tilting pad bearing on that end was changed to an offset-half design. The exhaust end bearing was changed to an optimized five-pad design. The bearing temperatures were reduced significantly and the vibration through the critical speeds and at operating speed were lowered so that both turbines currently run less than 1.0 mil continuously, with no subsynchronous vibration components.

REFERENCES

API Publication 684, 1996, "Tutorial on the API Standard Paragraphs Covering Rotor Dynamics and Balancing: An Introduction to Lateral Critical and Train Torsional Analysis and Rotor Balancing," First Edition, American Petroleum Institute, Washington, D.C.

Juvinall, R. C., 1967, *Engineering Considerations of Stress, Strain, and Strength*, New York, New York: McGraw Hill, Inc.

Young, W. C., 1989, *Roark's Formulas for Stress and Strain*, Sixth Edition, New York, New York: McGraw Hill, Inc.

ACKNOWLEDGMENTS

The authors wish to thank CONMEC, Inc., for the bulk of the actual engineering design of the turbine revamp. Hickham Industries, Inc., was also instrumental in developing the disk mounting procedures and the high-speed balancing. Koenig supplied a well designed turning gear with no problems. The bearings were supplied by Turbo Components and Engineering, Inc., and they also supplied Figure 6. The drafting skills of Fred Sandberg of FMSCO were important in producing accurate rotor drawings for modeling and making sure everything fit. We also thank the numerous other vendors involved, all working together toward a successful project conclusion.